Image Reconstruction in Three-Dimensional Magnetostatic Permeability Tomography

Manuchehr Soleimani and William R. B. Lionheart

School of Mathematics, The University of Manchester, Manchester M60 1QD, U.K.

Magnetostatic permeability tomography is an imaging technique that attempts to reconstruct the permeability distribution of an object using magnetostatic measurement data. The data for image reconstruction are external magnetic field measurements on the surface of the object due to an applied magnetostatic field. Theoretically, the normal and tangential components of the magnetic field in the surface uniquely define the internal isotropic permeability distributions. However, the inverse permeability problem is an ill-posed nonlinear problem. Regularization is needed for a stable solution. In this paper, we present a numerical method to solve the reconstruction problem in three dimensions using a regularized Gauss–Newton scheme. We have solved the forward problem using an edge finite-element method and we have employed an efficient technique to calculate the Jacobian matrix. The permeability of the object is assumed to be linear and isotropic. We present the reconstruction results for the permeability using synthetically generated data with additive noise.

Index Terms—**Edge finite-element method, inverse problems, magnetostatic permeability tomography.**

I. Introduction

MAGNETOSTATIC permeability tomography (MPT) is an imaging modality that is part of a larger family of magnetically coupled electromagnetic imaging techniques such as magnetic induction tomography (MIT) [8]. The magnetostatic fields are applied to the object. The primary magnetic field can be generated using a permanent magnet or an electromagnet such as a solenoid. The resulting magnetic field can be detected using a magnetometer, or for alternating magnetic field a detection coil. In this paper, we apply an alternating electric current to the excitation coil(s) and measure the induced voltages in sensing coils, which gives similar information to the data from tangential and normal components of the magnetic field. There are potential applications for MPT with magnetostatic fields in material inspection. For example, structural materials in reinforced concrete, often made of steel, are sometimes damaged due to ingress of corrosive solutions. This damage changes the magnetic permeability. An MPT system can give information about the steel bars inside of the concrete as well as reconstructing their number, shape, and position. In [7] and [16], an inductive scanner has been used to recover the conductivity and permeability of steel bars within a concrete structure. In this paper we focus on tomographic notion of a magnetostatic imaging system using the forward solution and Jacobian matrix, which can be described as a phenomenological method. Nonphenomenological methods as described in [13] (techniques that ignore the underlying physical process of the forward problem) also can be used for the inverse problem of MPT; as an example simple linear superposition used in [7].

There have been some studies to reconstruct permeability distribution using magnetostatic data. In [9] and [11], MPT reconstruction has been studied for the two-dimensional case. Wexlers's method [22] has been used to reconstruct the permeability distribution. This method shows very slow convergence and requires several hundred solutions of the forward problem, which makes the technique computationally very expensive, especially in three dimensions. A regularized one-step permeability reconstruction for simple geometry and with an analytical forward problem has been presented in [3]. Given the fact that the inverse problem in MPT is a nonlinear problem and there is not an analytical solution for the general form of the magnetostatic forward problem, the method proposed in [3] cannot be used in general. In this paper, we are proposing a regularized Gauss–Newton method. We incorporate *a priori* information in the regularization; the method is nonlinear and the convergence of method is known to be good for similar inverse problems [15]. Knowing the tangential component of the applied field and normal component of the measured field uniquely defines the permeability distributions for all possible excitations [20]. In practice, a finite set of external excitation and sensing coils (or the magnetic field sensors) can be used for the measurement configuration. The problem of the permeability reconstruction is then a nonlinear and ill-posed inverse problem. We explore the use of a standard Tikhonov regularization method to both low- and high-contrast permeability imaging. The purpose of this paper is to show use of a regularized and nonlinear reconstruction scheme to the MPT. The method has been widely used for a similar inverse problem in electrical impedance tomography (EIT) (see for example [15]). An edge finite-element method (EFEM) has been used to solve the magnetostatic problem formulated using the magnetic vector potential [1]. For the Jacobian matrix and the sensitivity analysis, an efficient adjoint field method has been used. We show the results of three-dimensional (3-D) permeability reconstruction for a numerically simulated MPT system.

II. Simulated MIT System

The simulated MIT system here is assumed to have eight coils, which are used for applying and detecting the magnetostatic fields. The coils have 0.04 m inner and 0.05 m outer diameter and 0.02 m length. The coils are arranged in a circular ring

Digital Object Identifier 10.1109/TMAG.2005.845158

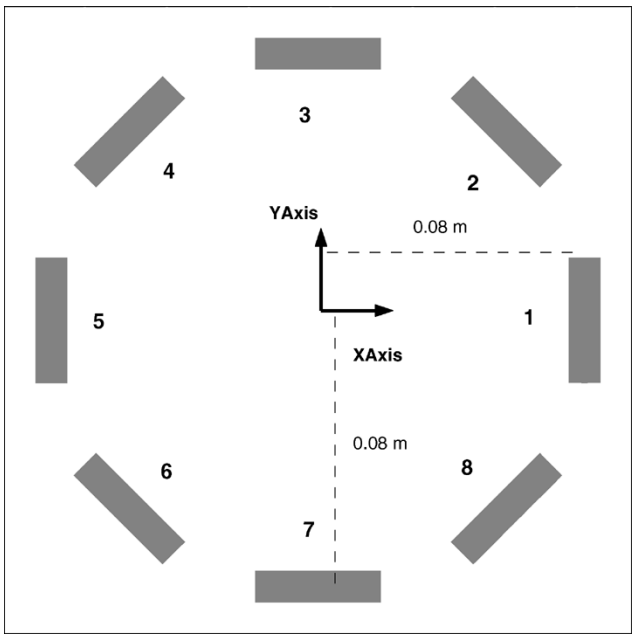

Fig. 1. Excitation and sensing coils, view from top.

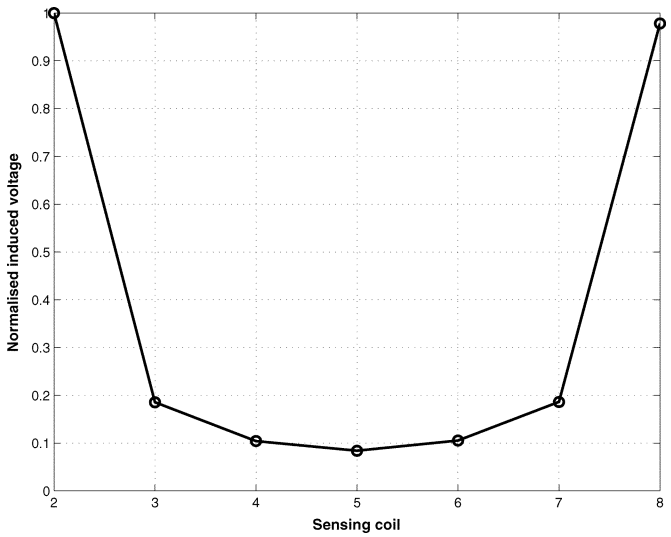

Fig. 2. Normalized induced voltage in coils 2–8 when the coil 1 is excited.

surrounding the object to be imaged. In this example the distance between center of two coils in opposite sides is 0.160 m, center of coils ring is at (0, 0, 0). Fig. 1 shows coil arrangement of the MIT system including eight coils. The system could have a magnetic shield, but in this paper the far field boundary condition $\mathbf{B}_n = 0$ is applied to the model and a magnetic shield has not been considered. The frequency of the applied current is 16 kHz, and for simplicity we use a 1 A/m current applied to the excitation coil. The region of interest for the permeability imaging is a cylinder with radius 0.07 m, length 0.10 m centered at (0,0,0), and has a relative permeability of 3 (we call it C1). Each coil is excited in turn and the induced voltages are measured in the remaining coils.

III. Forward Problem

The "forward problem" is to predict the measurement data given the permeability distributions, and given the applied current pattern and geometrical data. The interior magnetic fields are needed for the efficient computation of the Jacobian matrix, which will be described in the next section. The magnetostatic field can be formulated using edge-based finite element for the magnetic vector potential ($\mathbf{A}$) [2]. EFEM has the advantage of satisfying normal continuity of the magnetic field, so it handles multiply connected materials and jumps in permeability. Given $\mathbf{B} = \nabla \times \mathbf{A}$, then

$$\nabla \times (\nu \nabla \times \mathbf{A}) = \mathbf{J_s} \tag{1}$$

where $\nu = 1/\mu$. EFEM has some promising advantages compared with the more conventional nodal finite-element method. In EFEM, on a tetrahedral mesh a vector field is represented using a basis of vector valued functions. The natural boundary condition (normal component of magnetic field vanishes) is applied in far field. Galerkin's approximation to the governing equations using edge-element basis functions is

$$\int_{\Omega} (\nabla \times \mathbf{N} \nu \nabla \times \mathbf{A}) dv = \int_{\Omega_c} (\mathbf{N} \mathbf{J_s}) dv \tag{2}$$

where $\mathbf{N}$ is any linear combination of edge basis functions, $\mathbf{N}_{ij}$ associated with the edge between nodes i and j

$$\mathbf{N}_{ij} = L_i \nabla L_j - L_j \nabla L_i. \tag{3}$$

L_i is first-order nodal shape function, Ω is the entire region, and Ω_c is the current source region. In order to improve the convergence of the EFEM, we use an electric vector potential $\mathbf{T}_s$ to represent the current in excitation coil in which $\nabla \times \mathbf{T}_s = \mathbf{J}_s$ [17]. Incomplete Cholesky conjugate gradient (ICCG) has been successfully used to solve the linear system of (2) arising from the EFEM forward model without applying any gauge conditions. In the simulation, the number of tetrahedral elements was 69 804. The measured induced voltages (V) in sensing coils were calculated using

$$V = -i\omega \int_{\Omega_c} (\mathbf{A} \cdot \mathbf{J}_0) dv \tag{4}$$

where $\mathbf{J}_0$ is virtual unit current passing through the coil. In Fig. 2, the normalized induced voltage for coils $2, 3, \ldots, 8$ when coil 1 is excited is shown, the object is symmetric with respect to the coils $2, 3, \ldots, 8$ and the voltages are normalized with respect to the induced voltage in coil 2. An error in computation (about 1.5%) is difference between voltages of coils 2 and 8 as they are closest to the excitation coil. (The coils 2, 8 are in the same position with respect to coil 1 so ideally the calculated voltage for them must be the same.) The permeable object is the cylinder C1 and the rest of space has relative permeability 1.

We have developed a general eddy current and magnetostatic package written in Matlab for the forward problem. In [18], the forward problem for both magnetostatic and the eddy current

has been validated against experimental data as well as a commercial package called MAFIA (MAxwell's equations by the Finite Integration Algorithm).

IV. Sensitivity Analysis

There are a number of ways to model the excitation and measurement coils. As in any imaging system, the sensors must be modeled. Rather than modeling individual turns of copper wire, we will use a simplified model of a coil as a surface, (topologically at least) an open-ended cylinder. When used as an excitation coil, this surface carries a tangential current $\mathbf{J}_s$. This is equivalent to a surface that is perfectly conducting in one direction (angular for a cylinder) and an insulator in another (axial) direction, with each loop fed by a perfect current source. The excitation coil is modeled to give an accurate tangential $\mathbf{H}$. With a similar argument, the measured induced voltage in the exciting coil is the same as the measurement of the normal component of the magnetic field. There might be an external magnetic screen (shielding), which means that the normal component of $\mathbf{B}$ vanishes. In this study we assume a far field boundary condition, and where there is no shielding one would nevertheless need to apply far field boundary conditions to Maxwell's equations. The general form of the sensitivity analysis for Maxwell's equation has been studied in [6] and can be applied here. The sensitivity to the change in permeability of a region is proportional to an integral over the volume of the perturbing region of the inner product of the magnetic field density $\mathbf{B}$ from sensing and exciting coil [6], [10]. In [12], a more ideal model of the coils is considered to represent the measurement of the tangential $\mathbf{H}$ (for exciting coils) and normal $\mathbf{B}$ (as sensing coil) in the surfaces. In [12], a sensitivity formula has been derived for the general electromagnetic problem of MIT. Here, we are implementing numerically a form of the sensitivity formula using a magnetic vector potential formulation of the forward problem for MPT. Using the matrix of edge elements $[\mathbf{N}_e]$ in each element, the magnetic field $\mathbf{B}$ inside each element can be expressed as follows:

$$\mathbf{B} = [\nabla \times \mathbf{N}_e][\mathbf{A}_e] \tag{5}$$

where $[\mathbf{A}_e]$ are defined along edges and are the solution of the forward problem. The sensitivity term for each element is expressed as follows:

$$\frac{\partial V_{ij}}{\partial \mu_k} = \frac{i\omega\nu_0}{I_i I_j \mu_k^2}[\mathbf{A}_e^i]\left(\int_{\Omega_{ek}} [\nabla \times \mathbf{N}_e] \cdot [\nabla \times \mathbf{N}_e]^T dv\right)[\mathbf{A}_e^j]^T. \tag{6}$$

Equation (6) gives us sensitivity of the voltage induced in coil i when coil j is excited with respect to μ_k relative permeability of element k. Here, ν_0 is inverse of the permeability of free space, Ω_{ek} is the volume of element number k, and I_j and I_i are excitation current for coils. For first-order edge basis functions, the curl of the basis function is constant in each element so the integral in (6) is a constant and easy to calculate in each element. In Fig. 3, one can see a plot of the sensitivity when the excitation and sensing coils are coaxial (Coil 1 and 5) and are placed in two opposite sides of the object (two coils are centred at $(0.08, 0, 0)$ m and $(-0.08, 0, 0)$ m) and the background is the cylinder (C1).

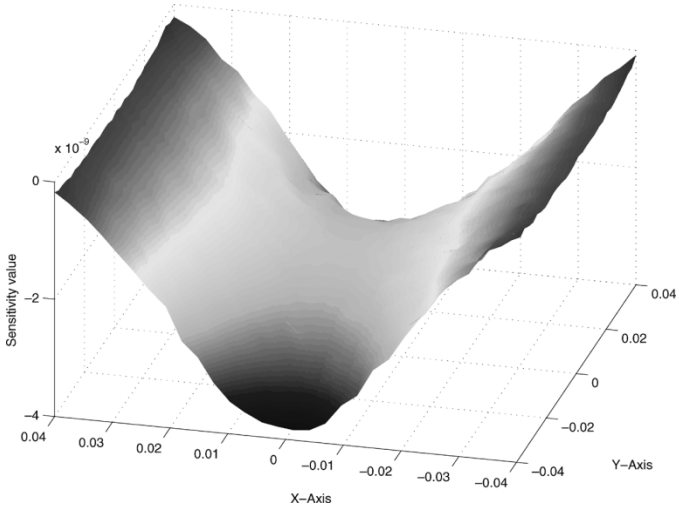

Fig. 3. Sensitivity plot for coils 1, 5 as excitation and sensing coils in plane $Z = 0$.

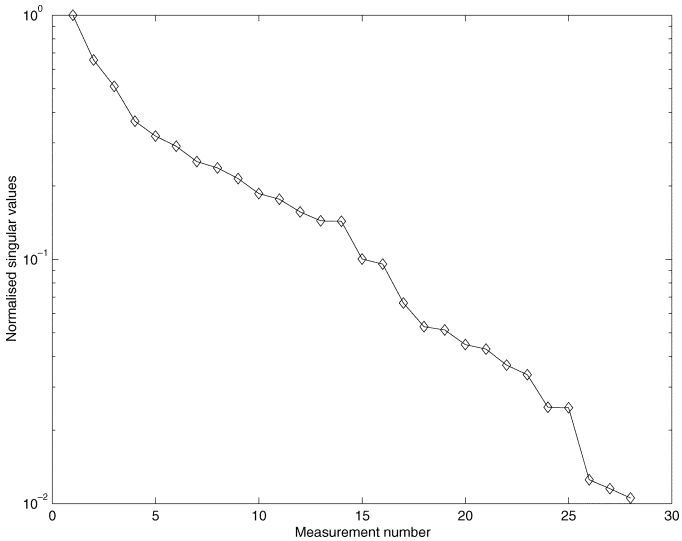

Fig. 4. Plot of the singular values for 28 independent measurements (normalized to the first and largest singular value).

Fig. 3 shows that the sensitivity is higher in the center and also near to the coils.

Each row of the Jacobian matrix is a sensitivity of one of the measured voltages to small change in each voxel's permeability value. In Fig. 4, one can see the singular values of the Jacobian matrix for the cylinder C1. The linear decay on a logarithmic scale shows that the inverse problem is severely ill posed. In this study, we use 28 mutual inductance measurements.

V. Image Reconstruction

Image reconstruction in MPT is an inverse medium problem. The Gauss–Newton method has been used for the image reconstruction for electrical imaging [14], [15], [19]. In [19], a regularized and one-step Gauss–Newton has been applied to the electrical conductivity imaging of MIT. In this paper, a general nonlinear regularized Gauss–Newton scheme is applied to an interesting and new imaging method, MPT. The forward solution provides a good understanding of the measurement process

and the Jacobian matrix provides partial knowledge of the inverse solution. The Gauss–Newton scheme provides a direction to improve the solution from a given point. The regularization methods enable us to include some prior knowledge of the measurement noise as well as prior knowledge of the permeability distribution, so the ill-posed inverse problem can be stabilized.

The algorithm starts with an initial permeability distribution. The forward problem is solved and the predicted voltages compared with the calculated voltages from the forward model. The permeability is then updated using the Jacobian matrix. The process is repeated until the measurement data agree with the calculated voltages from the finite-element model up to the measurement precision. The Jacobian matrix needs to be updated in each step, as the sensitivity map changes with change on background permeability.

Reformulation of the inverse problem to include prior information is known as regularization. A natural assumption will be that $||\mathbf{L}\mu||$ is not too large, which can mean the permeability is small, or slowly changing or smooth. Here, $\mathbf{L}$ is a matrix, typically a difference operator between neighboring voxels. We take $\mathbf{L}$ as first-order Laplacian operator in discrete form approximated by finite difference. Here, $\mathbf{L}(i,j) = -1$ for $i \neq j$ when two elements are neighbors (sharing at least one node) and $\mathbf{L}(i,i) = -\Sigma_j \mathbf{L}(i,j),\ i \neq j$. We solve this minimization problem by regularized Gauss–Newton, which is a compromise between the error of the mismatches between the measurement ($\mathbf{V}$) and the predicted voltages and the deviation from the prior information. The functional minimized is

$$||\mathbf{V} - \mathbf{F}(\mu)||^2 + \alpha^2 ||\mathbf{L}\mu||^2. \tag{7}$$

The minimization leads to linear steps, each of which is the Tikhonov regularized solution to the linearized problem

$$\delta\mu_{n+1} = (\mathbf{J}_n^T \mathbf{J}_n + \alpha^2 \mathbf{L}^T \mathbf{L})^{-1} (\mathbf{J}_n^T (\mathbf{V} - \mathbf{F}(\mu_n)) - \alpha^2 \mathbf{L}^T \mathbf{L} \mu_n). \tag{8}$$

For $n = 1$, this is a linear reconstruction algorithm. Here, $\mathbf{J}_n$ is the Jacobian calculated with the permeability μ_n, $\mathbf{V}$ is the vector of voltage measurements, and the forward solution $\mathbf{F}(\mu_n)$ is the predicted voltage from the forward model with permeability μ_n. The regularization matrix with a suitable regularization parameter α [15] penalizes extreme changes in permeability removing the instability in the reconstruction, at the cost of producing artificially smooth images. Here, α was chosen as 10^{-7}.

VI. Results and Discussion

For the first test, we inserted two bars with relative permeability of 4 into the cylinder C1 as a test phantom [see Fig. 5(a)]. Fig. 5(b) shows the reconstructed image from test phantom of Fig. 5(a). Fig. 5 is cross section of a 3-D image in a different level of Z direction.

For the second test, we inserted four high-permeability bars with relative permeability of 50 as shown in Fig. 6(a). Fig. 6(b) shows the reconstruction of this test phantom; the nonlinear reconstruction steps have been applied. The convergence plot shows the norm of the differences between measured and simulated voltages depicted in Fig. 7. In both cases, in order to avoid a so-called "inverse crime" we used two different meshes for generating simulated measurement data and for the forward solver

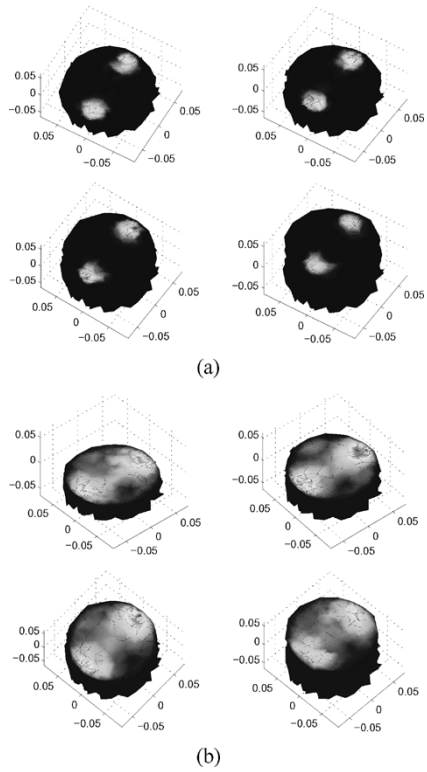

Fig. 5. Reconstruction of the test phantom in (a) can be seen in (b); the image is for different Z level of cylinder C1. (a) True object, two inclusions with permeability 4. (b) Reconstruction of object in (a).

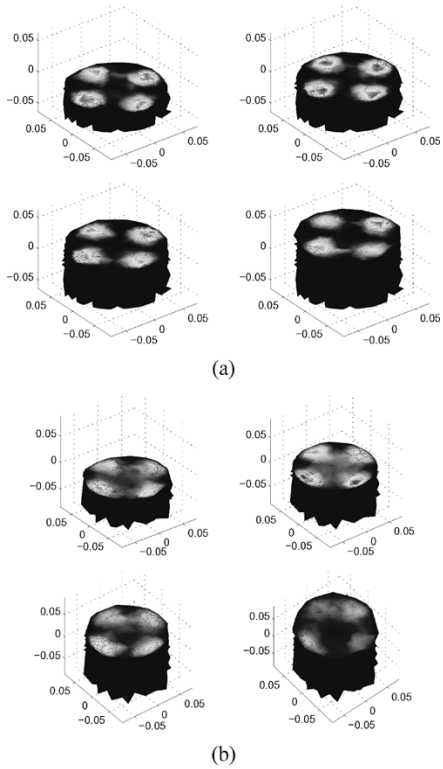

Fig. 6. Reconstruction of the test phantom in (a) can be seen in (b); the image is for different Z level of cylinder C1. (a) True object, four inclusions object with permeability 50. (b) Reconstruction of the object in (a).

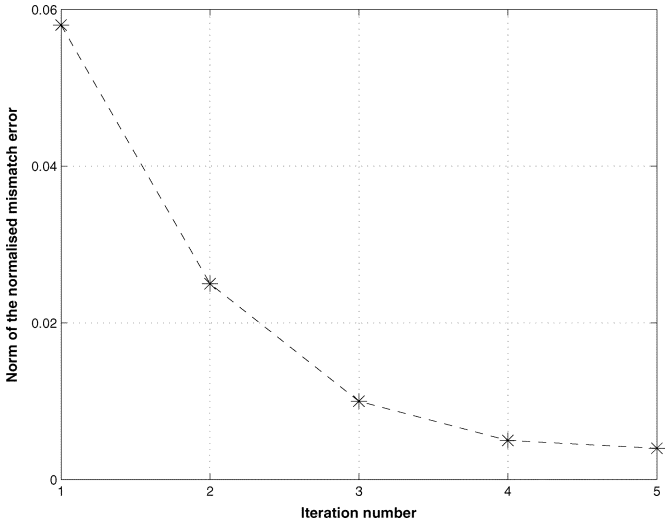

Fig. 7. Norm of the error between measured and simulated voltage (voltages are normalized to the voltage of free space).

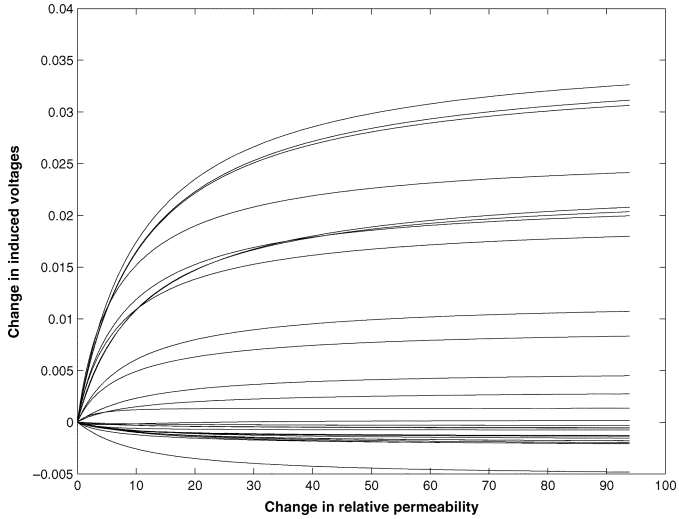

Fig. 8. Change in induced voltages (normalized to the voltage for free space) due to perturbation of permeability of a spherical object. Note the validity of a linear approximation for small changes and saturation for high changes.

and 2% Gaussian noise (2% of the mean value of the measurement voltages) was added to the data.

The image in the lower contrast case (Fig. 5) is more affected by the noise in the data as the changes on the voltages are small. For the higher permeability contrast case (Fig. 6) the measurement signals are higher, so if the objective is to recover shape and location of the high contrast inclusions the resulting images are better than the low contrast case in terms of spatial resolution. The maximum permeability values in reconstructed image in Fig. 5 is 3.89 and in Fig. 6 is 26.67. Although the spatial resolution of the reconstructed image in the case of high contrast permeability is good, the quantitative values of the permeabilities are not accurate. Reconstruction of the absolute value of the permeability in higher contrast is rather a more complicated task. Three major reasons for this are: the smoothing assumption of the Tikhonov regularization, the underdetermined nature of the problem, and the effect of measurement noise to the reconstructed quantitative values of the image (because of the saturation explained below). Quantitative accuracy of the image can be improved by additional constraints or *a priori* knowledge, or different regularization scheme such as total variation regularization [4]. A method has been introduced in [5] to use *a priori* information of location of inclusions and solving the inverse problem for reduced number of unknowns (here the values of permeabilities in all regions are the unknown; for example, for the image of Fig. 6 we have one background and four inclusions, so there are five unknowns to be recovered). Shape reconstruction methods can be used for two phase material reconstruction (for example, monotonicity based shape reconstruction of Tamburrino [21]), for a given low and high value of the permeability values. The third reason depends on the measurement accuracy. For high contrast, the sensitivity plot has saturation property, which means if we perturb a region and increase the permeability of the region, the resulting changes to the measurement voltages are linear with permeability changes, as we increase the permeability to the higher values the changes in the induced level out (see Fig. 8). This explains why it is hard to find the absolute permeability distribution in higher contrast case with noisy data.

Fig. 8 shows the change on induced voltages (for all 28 measurements), when the relative permeability of a spherical object (Radius 0.02 m and entered at (0.03, 0, 0) m), when the background is a cylinder C1. One can see that the voltages are changing linearly and saturation occurs for higher permeability changes. For this perturbation test, in order to avoid the discretization error we used a high mesh density (208 000 elements). As the voltage differences between two high contrast inclusions are very small, this difference will often be overshadowed by noises.

In Fig. 8 one region has been perturbed, and if we consider perturbation of more than one region (especially perturbation objects closed to each other) we can see the lack of superposition and the interferences between perturbed fields and perhaps more complicated pattern of the change in the measurement voltages. In test example of Fig. 6, the high-permeability inclusions are far from each other and the spatial resolution of reconstructed image is good. If two high-permeability inclusions are close to each other, as their magnetic field interferes with each other, the spatial resolution of the image will be degraded. Further studies are needed for high-contrast permeability imaging, especially when the absolute value of the permeability is required.

VII. Conclusion

This paper describes a regularized Gauss–Newton scheme for image reconstruction in 3-D magnetostatic permeability tomography. The reconstruction results are presented for high- and low-contrast permeability imaging. In the case of low contrast, one linear step is used to recover the permeability distribution. In the higher contrast case, the linear property does not hold and nonlinear reconstruction must be applied. Further study is needed to solve the inverse problem of high-contrast permeability, both in terms of regularization and quantitative accuracy of the reconstructed image.

REFERENCES

[1] O. Biro, "Edge element formulations of eddy current problems," *Comput. Meth. Appl. Mech. Eng.*, vol. 169, pp. 391–405, 1999.

[2] A. Bossavit, "Whitney forms: A class of finite elements for three-dimensional computations in electromagnetism," *Inst. Elect. Eng. Proc. A*, vol. 135, no. 8, pp. 493–500, Nov. 1988.

[3] R. Casanova, A. Silva, and A. R. Borges, "MIT image reconstruction based on edge-preserving regularization," *Physiol. Meas.*, vol. 25, pp. 195–207, 2004.

[4] T. F. Chan and X.-C. Tai, "Level set and total variation regularization for elliptic inverse problems with discontinuous coefficients," *J. Comput. Phys.*, vol. 193, pp. 40–66, 2003.

[5] H. Dehghani, B. W. Pogue, J. Shudong, B. Brooksby, and K. D. Paulsen, "Three-dimensional optical tomography: Resolution in small-object imaging," *Appl. Opt.*, vol. 42, no. 16, pp. 3117–3128, Jun. 2003.

[6] D. N. Dyck, D. A. Lowther, and E. M. Freeman, "A method of computing the sensitivity of the electromagnetic quantities to changes in the material and sources," *IEEE Trans. Magn.*, vol. 3, no. 5, pp. 3415–3418, Sep. 1994.

[7] P. A. Gaydecki, I. Silva, B. T. Fernandes, and Z. Z. Yu, "A portable inductive scanning system for imaging steel reinforcing bars embedded within concrete," *Sens. Actuators A, Phys.*, vol. 84, pp. 25–32, 2000.

[8] H. Griffiths, "Magnetic induction tomography," *Meas. Sci. Technol.*, vol. 12, no. 8, pp. 1126–1131, 2001.

[9] H. Igarashi, K. Ooi, and T. Honma, "Magnetostatic permeability tomography," presented at the Conf. Computation of Electromagnetic Fields (COMPUMAG) , Saratoga Springs, NY, 2003, Paper 43142.

[10] K. Hollaus, C. Magele, R. Merwa, and H. Scharfetter, "Fast calculation of the sensitivity matrix in magnetic induction tomography by tetrahedral edge finite elements and the reciprocity theorem," *Physiol. Meas.*, vol. 25, pp. 159–168, Feb. 2004.

[11] H. Igarashi, K. Ooi, and T. Honma, "A magnetostatic reconstruction of permeability distribution in material," in *Inverse Problems in Engineering Mechanics*, M. Tanaka, Ed., 2003, vol. IV, pp. 383–388.

[12] W. R. B. Lionheart, M. Soleimani, and A. J. Peyton, "Sensitivity analysis in 3D magnetic induction tomography (MIT)," in *Proc. 3rd World Congr. Industrial Process Tomography*, Banff, AB, Canada, 2003, pp. 239–244.

[13] Y. Li, L. Udpa, and S. S. Udpa, "Three-dimensional defect reconstruction from eddy-current NDE signals using a genetic local search algorithm," *IEEE Trans. Magn.*, vol. 40, no. 2, pp. 410–417, Mar. 2004.

[14] N. Polydorides and W. R. B. Lionheart, "A Matlab toolkit for three-dimensional electrical impedance tomography: A contribution to the electrical impedance and diffuse optical reconstruction software project," *Meas. Sci. Technol.*, vol. 13, pp. 1871–1883, 2002.

[15] N. Polydorides, "Image reconstruction algorithms for soft-field tomography," Ph.D. dissertation, Univ. Manchester Inst. Sci. Technol., Manchester, U.K., 2002.

[16] S. Quek, P. Gaydecki, B. Fernandes, and G. Miller, "Multiple layer separation and visualization of inductively scanned images of reinforcing bars in concrete using a polynomial-based separation algorithm," *Nondestruct. Test. Eval. Int.*, vol. 35, pp. 233–240, 2002.

[17] Z. Ren, "Influence of the R.H.S on the convergence behavior of the curl-curl equation," *IEEE Trans. Magn.*, vol. 32, no. 3, pp. 655–658, May 1996.

[18] M. Soleimani, W. R. B. Lionheart, C. H. Riedel, and O. Dossel, "Forward problem in 3D magnetic induction tomography (MIT)," in *Proc. 3rd World Congr. Industrial Process Tomography*, Banff, AB, Canada, 2003, pp. 275–280.

[19] M. Soleimani, W. R. B. Lionheart, A. J. Peyton, and X. Ma, "Image reconstruction in 3D magnetic induction tomography using a FEM forward model," in *Proc. 3rd World Congr. Industrial Process Tomography*, Banff, AB, Canada, 2003, pp. 252–255.

[20] E. Somersalo, D. Isaacson, and M. Cheney, "A linearized inverse boundary-value problem for Maxwell equation," *J. Comput. Appl. Math.*, vol. 42, pp. 123–136, 1992.

[21] A. Tamburrino and G. Rubinacci, "A new noniterative inversion method in electrical resistance tomography," *Inverse Problems*, vol. 18, pp. 1809–1829, 2002.

[22] A. Wexler, B. Fery, and R. Neuman, "Impedance-computed tomography algorithm and system," *Appl. Opt.*, vol. 24, pp. 3985–3992, 1985.

Manuscript received March 31, 2004; revised December 16, 2004.